Design and Implementation of a High-Efficiency Multiple Output Charger Based on the Time-Division Multiple Control Technique

Van-Long Tran, Hai-Nam Vu, Dai-Duong Tran, and Woojin Choi, *Member, IEEE*

***Abstract*—Multiple output converters (MOCs) are widely applied to applications requiring various levels of output voltages due to their advantages in terms of cost, volume, and efficiency. However, most of the conventional MOCs cannot regulate multiple outputs tightly and they can barely avoid the cross-regulation problem. In this paper, the recently developed time-division multiple control (TDMC) method, which can regulate all of the outputs with a high accuracy, is used for a multiple output battery charger based on the phase-shift full-bridge topology to simultaneously charge three batteries. The proposed charger is able to charge three different kinds of batteries or three of the same kind of battery in different state of charges (SOCs) independently and accurately with the constant current/constant voltage (CC/CV) charge method. As a result, the strict ripple specification of a battery can be satisfied for multiple battery charges without difficulty. In addition, the proposed charger exhibits a high efficiency since the soft switching of all of the switches during the entire charge process can be guaranteed. The operating principle of the converter and the design of the controller, including the state-space average modeling, will be detailed, and the validity of the proposed method is verified through experiments.**

***Index Terms*—Multiple output battery charger, phase shift full bridge, time-division multiple control, and zero-voltage switching–zero-current switching (ZVS–ZCS).**

I. Introduction

MULTIPLE output converters (MOCs) are widely applied in many applications such as the switching-mode power supplies (SMPSs) of personal computers, portable electronics, household equipment, multiple voltage power supplies, and telecommunication systems [1]–[3]. One of the more promising applications of MOCs would be multiple battery chargers due to its advantages in terms of cost, volume, efficiency, and space for installation.

However, most of the conventional MOCs are not able to regulate all of the outputs accurately and independently without the help of complex hardware and controllers, which makes them unable to satisfy the strict ripple specifications of charge applications [4]–[7]. In order to overcome the aforementioned disadvantages, several methods have been suggested in the literature [8]–[17]. One method is to apply pre- and postregulators to control the multiple outputs [8]–[12]. However, accurate control in each slave output can barely be achieved since it is difficult to exactly match the magnetic coupling at each output. Furthermore, this makes it difficult to analyze the circuit. As a result, the design of the controller becomes difficult due to the complicated regulation between the outputs.

Another method uses a controlled current source in the form of a fairly big inductor connected to each output through a switch on a time shared basis during one switching cycle [13]–[15]. However, since it requires a large inductor as a current source, the converter becomes bulky and expensive. In addition, the method is extremely difficult to implement and complex in terms of small signal modeling on account of the differences in time sharing at each output during the freewheeling period of the inductor current. As a result, cross-regulation problem is an inherent disadvantage of this method.

Other methods utilize a hybrid control to regulate the multiple outputs. In [16], two outputs are regulated by controlling the duty cycle and frequency of the switch. However, the number of converter outputs is limited to two and the regulation performance of each output is not good enough for the charge applications. In [17], the outputs are regulated independently based on multiple-band modulation and demodulation, which are operated by superposed sinusoidal pulsewidth modulation (PWM), pulse frequency modulation, and band-pass filtering. However, this method is very complex in terms of its control and the large filter required for each output increases the volume and decreases the efficiency of the converter.

Since all of the aforementioned methods are designed to control all of the outputs in one switching cycle, the cross regulation between the outputs is an inherent problem. In addition, this requires as many secondary windings in the transformer as the number of outputs in case of isolated converter topologies. The recently developed time-division multiple control (TDMC) method has been applied to multiple output chargers in order to overcome the drawbacks mentioned earlier [18], [19]. However, since the proposed topology in [18] was developed based on the double-ended forward converter, it is only suitable for small power applications due to the inherent limitation of the topology. In addition, the efficiency is not high enough since all the switches operate with hard switching and the duty cycle of the switch is limited less than 50% in order to reset the magnetizing current of the transformer. In this paper, a TDMC method based on the phase-shift full-bridge topology is proposed for multiple

Manuscript received September 25, 2015; revised February 13, 2016; accepted March 29, 2016. Date of publication April 7, 2016; date of current version November 11, 2016.

V.-L. Tran was with the Department of Electrical Engineering, Soong Soongsil University, Seoul 156-743, Korea. He is now with Lutronic Corp., Goyang-si 412-220, South Korea (e-mail: tranvanlong988@gmail.com).

H.-N. Vu, D.-D. Tran, and W. Choi are with the Department of Electrical Engineering, Soong Soongsil University, Seoul 156-743, Korea (e-mail: nam.vhn91@gmail.com; trandaiduong188@gmail.com; cwj777@ssu.ac.kr).

Color versions of one or more of the figures in this paper are available online at http//ieeexplore.ieee.org.

Digital Object Identifier 10.1109/TPEL.2016.2551723

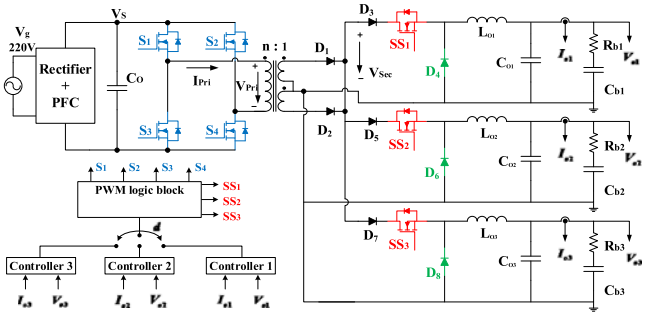

Fig. 1. Proposed multiple output charger based on TDMC method for three Li–Po batteries.

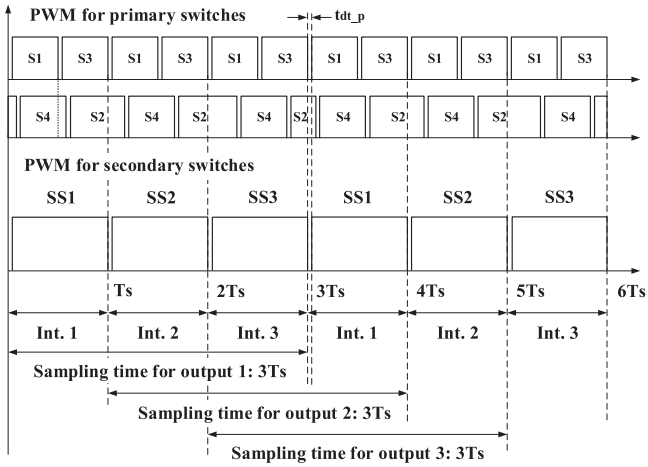

Fig. 2. PWM scheme for the primary and secondary switches of the proposed converter with TDMC method.

output charger applications to overcome the drawbacks of previous research. The major advantages of the proposed multiple output charger can be summarized as follows:

1) it offers an even degree of tight and independent regulation for each output, which is essential for multiple output charge applications;
2) it is simple in design and analysis and easy to model the circuit;
3) no cross-regulation problem exists among the outputs;
4) only one secondary winding of the transformer is required to regulate the multiple outputs if no isolation between the outputs is required;
5) zero-voltage switching (ZVS) turn-on can be achieved at all primary switches during the entire charge process;
6) zero-current switching (ZCS) turn-on and ZVS turn-off can be achieved at all the secondary switches with no additional circuit.

As a result, the proposed converter can be used for the higher power applications since it has been developed based on the full bridge topology and exhibits a high efficiency. The proposed multiple battery charger is able to charge a number of batteries at different state of charges (SOCs) by using constant-current and constant-voltage (CC/CV) charge modes, which is considered to be an efficient method to charge batteries [6], [20]. Since the TDMC method can control each output independently, the battery at each output can be charged independently by either the CC mode or the CV mode. As a result, three batteries can be charged simultaneously. In addition, it is possible to satisfy the strict ripple specifications of the batteries since the cross-regulation problem between the outputs does not exist. The circuit operation and modeling of the proposed topology will be detailed in the following sections. The effectiveness and feasibility of the proposed multiple output charger will be verified by experimental results.

II. Proposed MOC and Its Operation Principle

Fig. 1 shows the proposed multiple output charger based on the phase-shift full-bridge topology, including *R–C* models of the Li–Po batteries with the TDMC method. As shown in Fig. 1, the proposed converter is developed by modifying the conventional phase-shift full-bridge converter, where three different output circuits share the secondary windings of the transformer and an active switch (SS_1, SS_2, and SS_3) is added to each output to carry out the TDMC method. In addition, a diode is added in front of the secondary switch at each output to block the discharge current from the batteries with high voltage, while one battery is being charged.

Fig. 2 demonstrates an overview of the PWM scheme for the proposed converter with the TDMC method during the unbalanced load at each output in which t_{dt_p} is the dead time between the two switches in a leg at the primary side and the secondary switches at each output. As shown in Fig. 2, the PWM is performed at the switching frequency of f_s for the primary switches and at $f_s/3$ for each of the secondary switches. The proposed method is able to regulate all of the outputs in one sampling time ($3T_S$). Each output is controlled independently and precisely during one interrupt cycle T_S by way of a secondary switch. In one interrupt cycle, there is only one secondary switch turned on to allow the primary side to control each output by shifting the phase between the leading-leg and lagging-leg switches. Similarly, another output is regulated in the next interrupt cycle. Hence, all of the outputs are regulated properly in one sampling time ($3T_S$). In the proposed method, since each output is regulated independently within one interrupt cycle (T_S), no cross-regulation problem exists. Thus, it is possible to provide an even degree of tight regulation for all of the outputs.

As demonstrated in Fig. 3, the primary side operates as a conventional phase-shift full-bridge converter and the TDMC method is implemented at the secondary side through the active switches. The conventional phase shift PWM scheme is used to achieve ZVS at all of the primary side switches by shifting the phases of the gate signals between leading-leg switches (S_1 and S_3) and lagging-leg switches (S_2 and S_4) [21]. Since, in the proposed converter, the primary side operates at the switching frequency of *fs* and each of the secondary sides operates at the switching frequency of $fs/3$ to achieve the TDMC method, each secondary output circuit operates sequentially with the help of the additional switches (SS_1, SS_2, andSS_3) at each switching

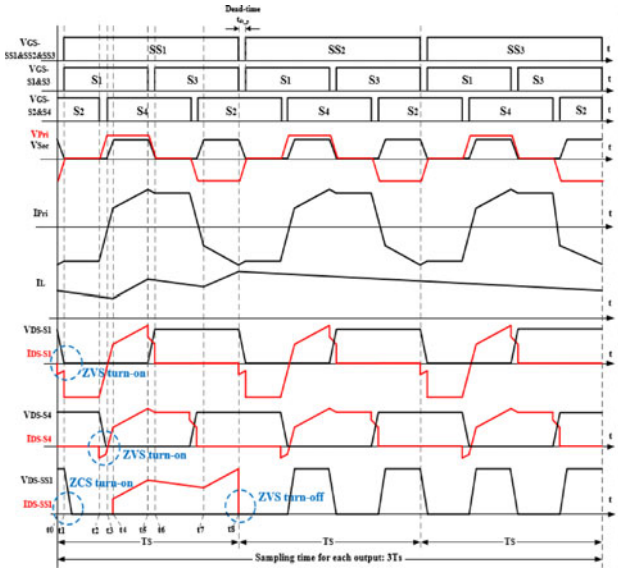

Fig. 3. Key waveforms at the primary and secondary sides of the proposed converter in the steady state.

cycle (T_S) of the primary side. Hence, only the operation of the primary circuit and one secondary circuit out of the three is described since others operate in the same manner. In order to simplify the analysis of the circuit operation, some assumptions are made as follows. All of the switches and diodes are ideal except for the output capacitor and the internal anti-parallel diode of the switches, and all of the other parasitic components are neglected. The operation principle of the proposed converter at each output under the continuous conduction mode (CCM) consists of the following nine modes:

1) *Mode 1* [t_0, t_1) *[see Fig. 4(a)]:* Prior to t_0, switches S_2 and S_3 are conducting and the power is transferred from the primary side to the secondary side through the secondary switch SS_3. After the switch S_3 is turned off at $t = t_0$, the primary current $I_{\rm Pri}$ charges the output capacitance of switch S_3 and discharges the output capacitance of switch S_1. At $t = t_1$, the voltage of switch S_1 is decreased to zero, resulting in the conduction of its body diode; hence, the ZVS condition is achieved for switch S_1. Meanwhile, the voltage of switch S_3 is increased to the input voltage $V_{\rm S}$ and the switch current is decreased to zero. The transformer secondary voltage $V_{\rm Sec}$ becomes zero at $t = t_1$ and the output inductor current $I_{\rm L}$ flowing through diode D_4 ramps down with a slope of V_o/L_{o1}.
2) *Mode 2* [t_1, t_2) *[see Fig. 4(b)]:* During this interval, the primary current $I_{\rm Pri}$ freewheels through the switch S_1 and switch S_2 and no power is delivered to the load. The secondary switch $\rm SS_1$ is turned on at t_1, and the voltage across it starts to decrease to zero. However, the current of the switch $\rm SS_1$ remains at zero until the primary current $I_{\rm Pri}$ reverses its direction and rise to reach the reflected output inductor current at t_4. Hence, the ZCS turn-on of the secondary switch $\rm SS_1$ is achieved during this mode. The output inductor current $I_{\rm L}$ flowing through diode D_4 ramps down with a slope of V_o/L_{o1}.
3) *Mode 3* [t_2, t_3) *[see Fig. 4(c)]:* At $t = t_2$, the switch S_2 is turned off, the primary current $I_{\rm Pri}$ starts to charge the output capacitance of switch S_2 and discharge the output capacitance of switch S_4. Hence, the voltage of switch S_2 is increased to the input voltage V_S and the switch current is decreased to zero. The transformer secondary voltage $V_{\rm Sec}$ remains at zero and $I_{\rm L}$ keeps ramping down with a slope of V_o/L_{o1} in this mode. No power is delivered to the output in this mode, and it is considered as the duty cycle loss.
4) *Mode 4* [t_3, t_4) *[see Fig. 4(d)]:* At $t = t_3$, the voltage of switch S_4 is decreased to zero, resulting in the conduction of its body diode, thereby achieving the ZVS condition. The transformer secondary voltage $V_{\rm Sec}$ starts to increase when switch S_4 is turned on at $t = t_3$. The output inductor current $I_{\rm L}$ keeps ramping down with a slope of V_o/L_{o1} and reaches its minimum value at $t = t_4$. This mode is also considered as the duty cycle loss.
5) *Mode 5* [t_4, t_5) *[see Fig. 4(e)]:* At t_4, the secondary switch $\rm SS_1$ starts to conduct since it was already turned on with ZCS during the mode 1. The output inductor current starts to ramp up with a slope of $(V_{\rm Sec} - -V_o)/L_{o1}$ until $t = t_5$. The primary current $I_{\rm Pri}$ is equal to the reflected output inductor current $I_{L_{o1}}/n$, and the power is delivered to the secondary through switches S_1 and S_4. Since the operation principle of the primary side is symmetrical during one switching period T_s, the circuit operation of the other half of a switching period (modes 6 and 7) is the same as that of the first half of a switching period (modes 1 to 5).
6) *Mode 6* [t_5, t_6) *[see Fig. 4(f)]:* The primary switch S_1 is turned off at t_5. The primary current $I_{\rm Pri}$ charges the output capacitance of switch S_1 and discharges the output capacitance of switch S_3. Therefore, the voltage of switch S_3 is decreased to zero resulting in the conduction of its body diode. Hence, the ZVS turn-on condition for the switch S_3 is achieved, while the voltage of switch S_1 is increased to the input voltage V_S. The current of switch S_1 is decreased to zero and the output inductor current $I_{\rm L}$ starts to ramp down with a slope of V_o/L_{o1}.
7) *Mode 7* [t_6, t_7) *[see Fig. 4(g)]:* At $t = t_6$, the switch S_3 is turned on with ZVS. The primary current $I_{\rm Pri}$ freewheels through switch S_3 and switch S_4, and no current flows through switches S_1 and S_2 during this mode. As a result, the transformer secondary voltage $V_{\rm Sec}$ remains at zero and it increases to V_S/n when switch S_2 turns on. The output inductor current I_L ramps down with a slope of V_o/L until $t = t_7$. During this mode, the switch S_2 achieves ZVS turn-on by the same principle applied to the switch S_4 as already explained in the mode 3 and mode 4.
8) *Mode 8* [t_7, t_8) *[see Fig. 4(h)]:* The output inductor current starts to ramp up with a slope of $(V_{\rm Sec}–V_o)/L_{o1}$ until $t = t_8$. The primary winding current $I_{\rm Pri}$ is equal to the reflected output inductor current $I_{L_{o1}}/n$. In this mode, the power is delivered to the secondary through switches S_2, S_3 and $\rm SS_1$. At $t = t_8$, both switch S_3 and $\rm SS_1$ are turned off and the current of the secondary switch $\rm SS_1$ is decreased to zero immediately. Since the current is

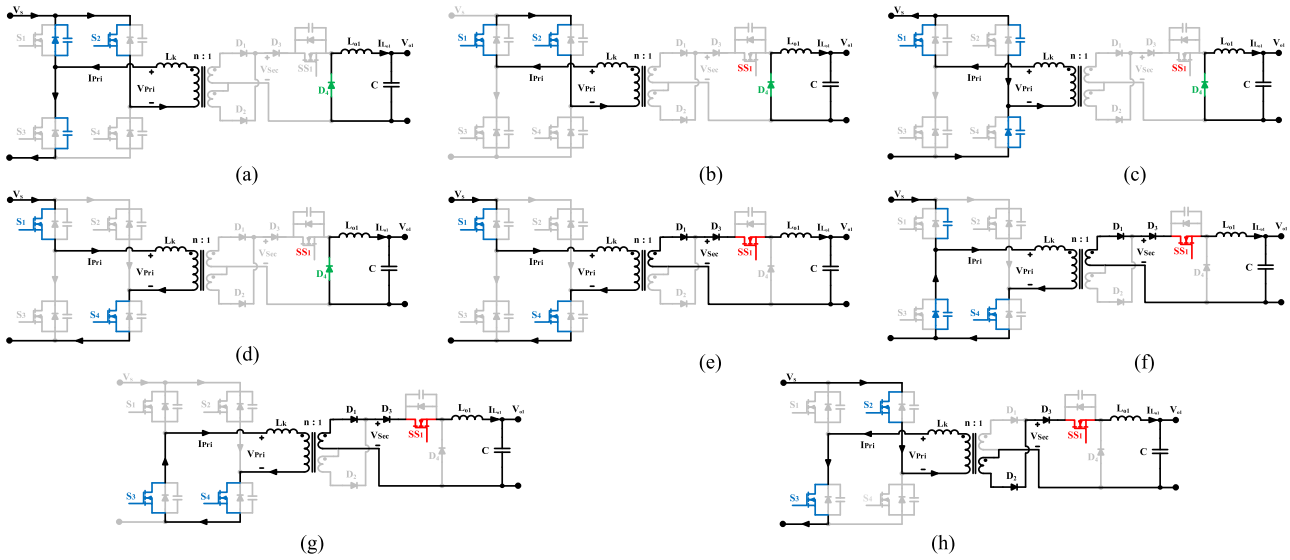

Fig. 4. Operation modes of the proposed multiple output charger in one sampling time ($3T_S$) at each output. (a) Mode 1 $[t_0 - t_1)$, (a) Mode 2 $[t_1 - t_2)$, (c) Mode 3 $[t_2 - t_3)$, (d) Mode 4 $[t_3 - t_4)$, (e) Mode 5 $[t_4 - t_5)$, (f) Mode 6 $[t_5 - t_6)$, (g) Mode 7 $[t_6 - t_7)$, (h) Mode 8 $[t_7 - t_8)$

freewheeling in the primary side and no voltage is applied to the secondary winding of the transformer, the voltage across the SS_1 is maintained at zero until the switch S_4 turns on and the ZVS turn-off of the secondary switch SS_1 is achieved.

The second and third outputs operate in the same manner as that already described in Mode 1 through Mode 8.

In order to achieve the ZVS turn-on for all primary switches during the overall charge process, sufficient energy for the soft switching and a suitable dead-time are essential. To guarantee the soft switching condition, the total inductive energy ($\mathrm{E_L}$) stored in the primary circuit should be larger than the total capacitive energy (E_C) of the switches during modes 1 and 4 [see Fig. 4(a) and (d)]. The total capacitive energy in a switching leg can be expressed as (1) by using the output capacitance of switch C_{OSS} and the input voltage V_s. As shown in mode 1, the leakage inductance, the magnetizing inductance, and the reflected output inductance all contribute to the available inductive energy for ZVS. Hence, the total inductive energy available for the ZVS of the leading-leg switches can be expressed as (2).

However, in the mode 3, since the voltage of the transformer is clamped to zero and the output inductor current freewheels through the diode D_4 at the secondary side, only the energy stored in the leakage inductance is used for the ZVS of the lagging-leg switches as (3)

$$E_C = C_{\mathrm{OSS}} \times V_S^2 \tag{1}$$

$$E_{L\_\mathrm{Lead}} = \frac{1}{2}L_M I_{M,pk}^2 + \frac{1}{2}LI_{L,\max}^2 + \frac{1}{2}L_k\left(I_{M,pk} + \frac{I_{L,\max}}{n}\right)^2 \tag{2}$$

$$E_{L\_\mathrm{Lag}} = \frac{1}{2}L_k\left(I_{M,pk} + \frac{I_{L,\min}}{n}\right)^2 \tag{3}$$

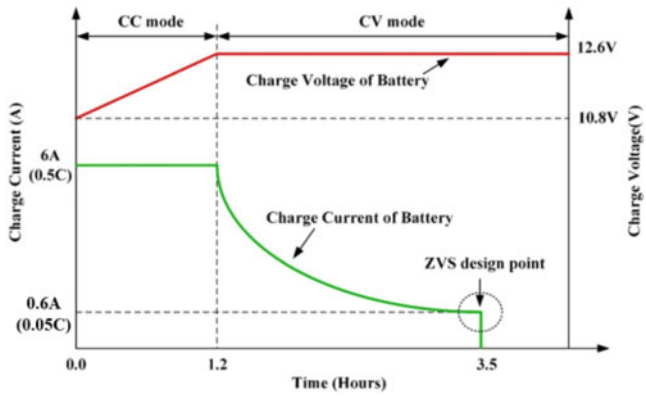

Fig. 5. Charge current and voltage characteristics of the battery and the ZVS design point of the proposed multiple output charger.

where L_M and I_M are the magnetizing inductance and magnetizing current of the transformer, respectively. As shown in (2) and (3), the required inductive energy for the ZVS of the leading switches is larger than that of the lagging-leg switches. Thus, the magnetizing and leakage inductances of the transformer should be designed to guarantee the ZVS of the lagging-leg switches at the minimum output load in order to guarantee the ZVS condition for all of the primary switches during the overall charge process. As shown in Fig. 5, the inductive components of the transformer need to be calculated based on the charge current at the end of the CV-mode charge [0.1 C (1.2 A)] [6], [7].

III. State-Space Average Modeling of the Proposed Charger for CC/CV Charge Operation

As shown in Fig. 1, since the three secondary circuits have the same structure, the same control method can be applied to each secondary circuit in a time-shared basis. Thus, the

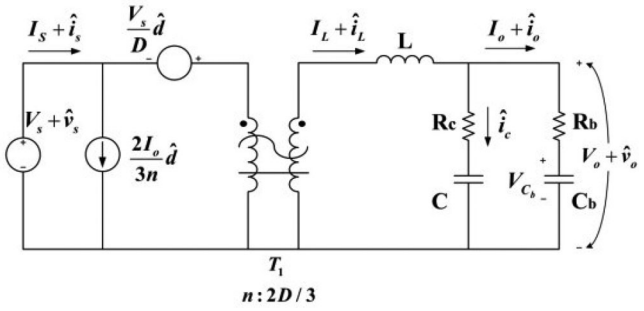

Fig. 6. State space average model of the proposed multiple output charger for each output with an *R–C* battery model.

control-to-output transfer function for only one secondary circuit needs to be derived. The battery is modeled by a resistor connected in series with a capacitor $C_{\rm b}$ having an initial voltage of V_{C_b} [22], [23]. The state space average model of the proposed multiple charger at each output including the *R–C* equivalent circuit model of Li–Po battery is shown in Fig. 6, where $D = 1/2 - -\vartheta/180^o$ (the effective duty cycle), and ϑ is the phase shift between the leading leg and lagging leg switches. By using KCL and KVL for the equivalent circuit during the phase shift and non-phase shift times between the leading leg and lagging leg, respectively, the state-space-averaged equations for the proposed charger at each output can be obtained as (4) to (8) [24], [25]

$$3L\frac{d\bar{i}_L}{dt} = 2\bar{d}\left(\frac{\bar{v}_s}{n} - \bar{v}_o\right) - (3-2\bar{d})\bar{v}_o \tag{4}$$

$$\bar{i}_L = \bar{i}_c + \bar{i}_o \tag{5}$$

$$\bar{i}_c = C\frac{d(\bar{v}_o - \bar{i}_c R_c)}{dt} \tag{6}$$

$$\bar{v}_o = \frac{1}{C_b}\int \bar{i}_o dt + \bar{i}_o R_b \tag{7}$$

$$\bar{i}_s = \frac{2}{3}\times\frac{\bar{d}}{n}\bar{i}_L. \tag{8}$$

By perturbing and linearizing the earlier averaged equations (4) to (8), the steady-state equations can be found as (9) to (11) based on the dc terms, and the small-signal-model equations can be found as (12) to (16) based on the ac terms

$$V_o = \frac{2}{3}\times\frac{D}{n}V_s \tag{9}$$

$$V_o = R_b I_o + V_{C_b} \tag{10}$$

$$I_s = \frac{2}{3}\times\frac{D}{n}I_o = \frac{2}{3}\times\frac{D}{n}I_L \tag{11}$$

$$3L\frac{d\hat{i}_L}{dt} = 2\frac{V_s}{n}\hat{d} + 2\frac{D}{n}\hat{v}_s - 3\hat{v}_o \tag{12}$$

$$\hat{i}_L = \hat{i}_c + \hat{i}_o \tag{13}$$

$$\hat{i}_c = C\frac{d(\hat{v}_o - \hat{i}_c R_c)}{dt} \tag{14}$$

$$\hat{v}_o = \frac{1}{C_b}\int \hat{i}_o dt + R_b\hat{i}_o \tag{15}$$

$$\hat{i}_s = \frac{2}{3n}(D\hat{i}_o + I_o\hat{d}). \tag{16}$$

In the CCM, the output inductor and the output capacitor of the proposed charger can be designed by using (17) and (18) based on the large-signal equations

$$L = \frac{V_O(3-2D_{\min})T_s}{2I_{o\_\min}} \tag{17}$$

$$C = \frac{3(3-2D_{\min})T_s^2 V_o}{8L\Delta V_o} \tag{18}$$

where $D_{\min}$ is the minimum effective duty cycle, $I_{o\_\min}$ is the minimum output current, and DV_o is the output voltage ripple. In the design of the output inductor, the cut-off charge current of the Li–Po batteries is used to guarantee the CCM operation of the charger during the entire charge process. Then, the output capacitor can be selected by using the output inductance value and the output voltage ripple values.

Since the proposed multiple output charger charges three Li–Po batteries by using constant current (CC) and constant voltage (CV) charge modes, it is necessary to derive the control-to-output current and control-to-output voltage transfer function for each output. By taking the Laplace transformation of (12) to (16), the resulting equations (19) to (21) can be obtained

$$\hat{i}_L = \frac{2\frac{V_s}{n}\hat{d} + 2\frac{D}{n}\hat{v}_s - 3\hat{v}_o}{3sL} = \hat{i}_c + \hat{i}_o \tag{19}$$

$$\hat{i}_c = sC(\hat{v}_o - \hat{i}_c R_c) \tag{20}$$

$$\hat{v}_o = \left(R_b + \frac{1}{sC_b}\right)\hat{i}_o \tag{21}$$

The control-to-output voltage transfer function of the proposed multiple output charger can be obtained as (22) by substituting (9), (19), and (20) into (21)

$$G_{vd}(s) = \left.\frac{\hat{v}_o}{\hat{d}}\right|_{\hat{v}_s=0} = \frac{V_o}{D}\times\frac{(1+a_1 s)(1+a_2 s)}{s^3 b_3 + s^2 b_2 + s b_1 + 1} \tag{22}$$

where $a_1 = R_b C_b, a_2 = R_c C, b_1 = R_c C + R_b C_b$, $b_2 = LC + LC_b + R_b R_c C C_b$, and $b_3 = R_b L C C_b + R_c L C C_b$.

Due to the huge capacitance value in the equivalent circuit model of the battery, the voltage variation at C_b during a small period of time can be neglected. Then, (21) can be rewritten as (23) as follows:

$$\hat{v}_o \cong R_b \times \hat{i}_o. \tag{23}$$

The control-to-output current transfer function of the proposed multiple output charger can be obtained as (24) by substituting (22) into (23)

$$G_{id}(s) = \left.\frac{\hat{i}_o}{\hat{d}}\right|_{\hat{v}_s=0} = \frac{V_{C_b} + I_o R_b}{D R_b}\times\frac{(1+a_1 s)(1+a_2 s)}{s^3 b_3 + s^2 b_2 + s b_1 + 1} \tag{24}$$

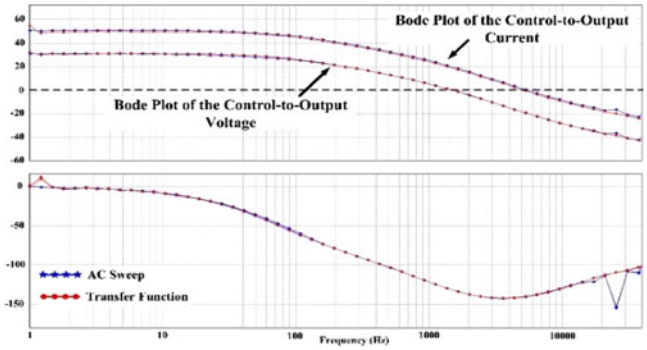

Fig. 7. Bode plot of control-to-output transfer functions drawn by ac sweep and transfer function block in PSIM for each output.

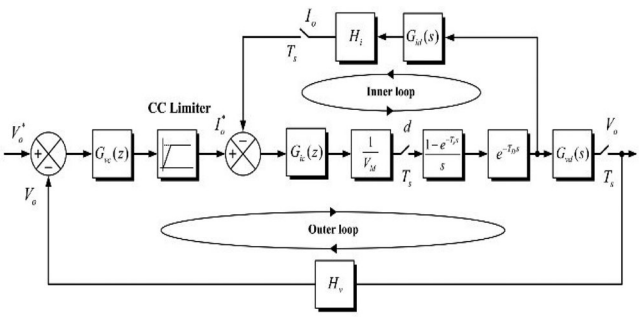

Fig. 8. Block diagram of the dual control loop for each output.

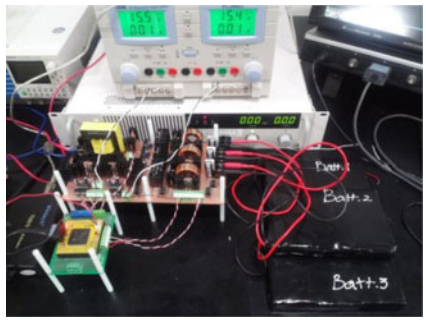

Fig. 9. Experimental circuit of the proposed converter with three Li–Po batteries.

TABLE I
SPECIFICATION OF THE PROPOSED MULTIPLE OUTPUT CHARGER

P_o	Power rating	250 W
V_S	Input voltage	380–400 dc
V_{o1}, V_{o2}, and V_{o3}	CV-mode voltage	12.6 V
I_{o1}, I_{o2}, and I_{o3}	CC-mode current	6 A (0.5 C)
R_b	Equivalent series resistance of the Li–polymer battery	0.116 Ω
C_b	Equivalent capacitance of the Li–polymer battery	21 500 F
ΔV_{o1}, ΔV_{o2}, and ΔV_{o3}	Output voltage ripple	$<2\%$ (252 mV)
ΔI_{o1}, ΔI_{o2}, and ΔI_{o3}	Output current ripple	$<5\%$ (0.6A)

IV. DESIGN OF THE DUAL-LOOP CONTROLLER FOR THE CC/CV CHARGE OF THE PROPOSED CHARGER

In order to verify the validity of the transfer function derived for the design of the controller in the previous section, Bode plots of the circuit using both the ac sweeping function and the transfer function block are drawn by PSIM as shown in Fig. 7. The results are well matched, which verifies the validity of the transfer function of the proposed charger. As shown in Fig. 7, both of the Bode plots of the control-to-output transfer functions have enough phase margin at the crossover frequency, and the gain slope in the high frequency range is enough to eliminate the switching noise. Then, it is necessary to put one pole at the origin to enhance the gain in the low frequency range, and one zero at the desired crossover frequency to make the closed-loop stable. Thus, the PI controller can be used for both voltage and current control of the proposed multiple output charger.

In this application, the CC/CV-mode charge is implemented by using a dual loop control where the inner control loop serves for the output current control and the outer loop serves for the output voltage control as shown in Fig. 8. The output voltage $V_{\rm o}$ is detected and compared with the reference voltage V_o*. Then, an error signal is generated and amplified to generate the current reference I_o*. Since the charge control starts with the constant current control at the beginning, the current reference should be limited to an appropriate value (6 A, 0.5 C in this case) to ensure safe charging of the battery. Then, the current reference I_o* is compared with the measured output current to generate an error signal, which is transmitted to the current controller. The output of the current controller is then compared with the triangular waveform V_M to generate PWM signals for the switches. In the design of the dual loop controller, the inner control loop requires a higher bandwidth, which is typically five to ten times faster than that of the outer loop, to guarantee that the inner loop will not affect the outer loop performance [26], [27]. The transfer functions of the closed loop control for the output current and output voltage in the z-domain are found as in (25) and (26), respectively

$$T_i(z) = G_{ic}(z) \times G_{id}(z) \times H_i \tag{25}$$

$$T_v(z) = G_{vc}(z) \times G_{vd}(z) \times H_v \tag{26}$$

where

$$G_{id}(z) = Z\left\{\frac{1-e^{-T_s s}}{s} \times e^{-T_d s} \times G_{id}(s)\right\}$$
$$G_{vd}(z) = Z\left\{\frac{1-e^{-T_s s}}{s} \times e^{-T_d s} \times G_{vd}(s)\right\}$$

where $G_{ic}(z)$ is the current loop compensator, $G_{vc}(z)$ is the voltage loop compensator, $(1-e^{-T_S S})/s$is the zero-order hold,$e^{-T_d s}$ is the computational delay, H_v is the voltage feedback gain, and H_i is the current feedback gain.

V. EXPERIMENTAL RESULTS AND DISCUSSION

Fig. 9 shows a prototype of the proposed multiple output charger with the specification shown in the Table I and its implementation details can be found in the Table II. The operation

TABLE II
IMPLEMENTATION DETAILS OF THE PROPOSED CONVERTER

f_S	Switching frequency Inductor	100 kHz
L_{o1}, L_{o2}, and L_{o3}	Changsung Core, CH330125 Number of Turns: 47 AWG 18	280 μH
C_{o1}, C_{o2}, and C_{o3}	Electrolytic capacitor Samyoung, KMG 1023	35 V, 1000 μF
S_1, S_2, S_3, and S_4	IGBT ST, STGB10NC60KD MOSEFT	600 V, 10 A
SS1, SS2, and SS3	Fairchild, FQP9N08	80 V, 9 A
D_1, D_2, D_3, D_4, D_5, D_6, D_7, and D_8	Diode ST, STPS10120C	120 V, 10 A
Transformer	Changsung Core, ES4117A AWG 25	$N_p/N_s = 60/7$

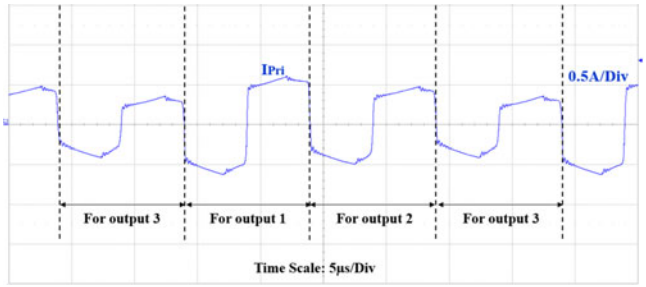

Fig. 10. Primary current waveform of the transformer with unbalanced load at each output.

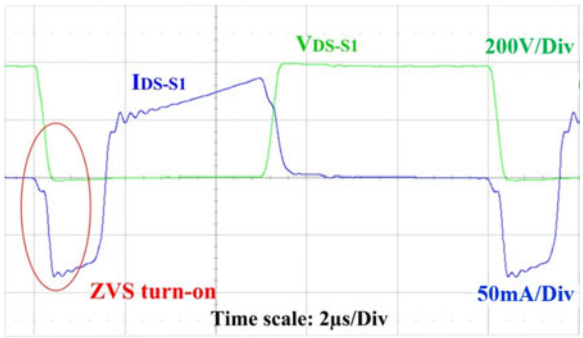

Fig. 11. ZVS turn-on of switch S_1 at the minimum load of 22.7 W.

and control of the proposed multiple charger are verified by simultaneously charging three Li–Po battery packs in different SOCs. The Li–Po battery pack configuration is 3S3P, meaning that three cells are connected in series and three strings of these are connected in parallel. For the control of the proposed charger a digital signal processor (DSP), TMS320F28335 from TI, was used to achieve the high speed calculations and switching.

Fig. 10 shows the primary current waveform of the transformer with unbalanced load at each output. It is shown in the figure that the duty and the amplitude of the primary current change continuously at each switching cycle in order to regulate each output separately.

Figs. 11 and 12 show the voltage and current waveforms of the switches S_1 and S_4 with minimum load (22.7 W) at the end

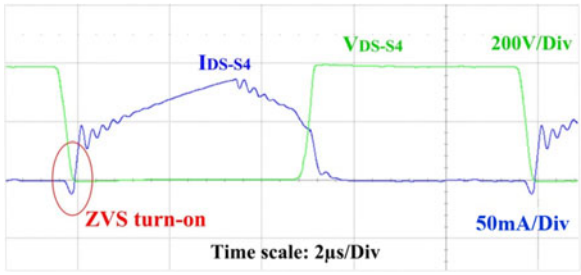

Fig. 12. ZVS turn-on of switch S_4 at the minimum load of 22.7 W.

of the CV charge. It is clearly shown in Fig. 11 and 12 that ZVS turn-on of switches S_1 and S_4 is successfully achieved. Since ZVS turn-on of the switches S_2 and S_3 can also be achieved at in the same fashion, ZVS turn-on of all the primary switches can be achieved during the entire charge process.

Fig. 13 shows the ZCS turn-on and ZVS turn-off waveforms of a secondary switch SS_1 when the output power is 22.7 and 226.8 W, respectively. The worst condition for the soft switching of secondary switch SS_1 is made when the output power at each output is maximum (226.8 W) since the effective duty becomes maximum and the minimum time is provided to maintain the switch current and the switch voltage at zero to achieve ZCS turn-on and ZVS turn-off, respectively. Since the soft switching of the secondary switch SS_1 is successfully performed both with light load [see Fig. 13(a)] and heavy load [see Fig. 13(b)], it can be achieved during the entire charge process.

Fig. 14 shows the inductor current waveforms at each output of the proposed charger. As shown in this figure, only one of the secondary switches is turned on to regulate each of the outputs independently and tightly. It can be observed from Figs. 15 and 16 that the proposed charger with the TDMC method satisfies the output ripple specification of the Li–Po batteries during the entire charge process. The voltage ripple is less than 2% (<0.252 V) and the current ripple is less than 5% (<0.6 A). Both of these are lower than the maximum allowable ripple values suggested by the battery manufacturer as specified in Table I [4]–[7].

Fig. 17 shows the experimental waveforms of the proposed multiple charger when the load varies from 50% to 100% of the rated load at the third output, while a 100% load is applied to the first and second outputs. The load variation at the third output only causes a small transient on the voltage regulation of the third output. This verifies that no cross-regulation problem exists in the proposed charger with the TDMC method.

Figs. 18 and 19 show the charge current and charge voltage profiles of three Li–Po batteries in different SOCs being charged by the proposed multiple output charger. It is demonstrated that the proposed converter and the TDMC method work properly to charge the three batteries. No cross regulation is observed even in the case where each of the outputs works in different charge modes.

Fig. 20 shows an efficiency plot of the proposed charger at each input voltage when the load varies from 25 to 250 W. The

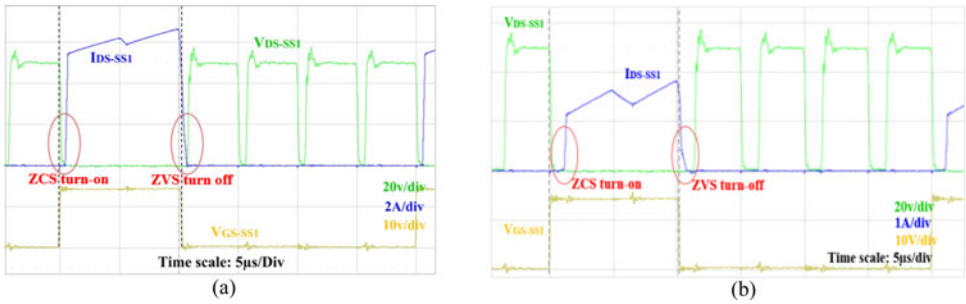

Fig. 13. ZCS turn-on and ZVS turn-off waveforms of the secondary switch SS_1. (a) When the output power is 22.7 W and (b) when the output power is 226.8 W.

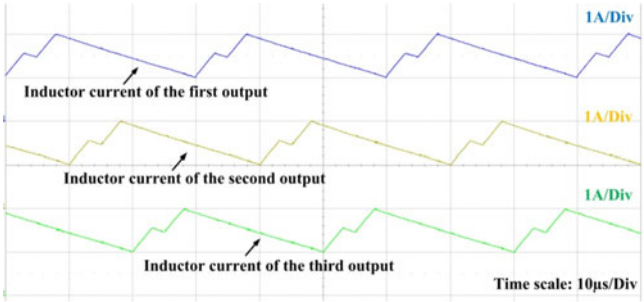

Fig. 14. Output inductor current waveforms of the proposed multiple output charger at each output.

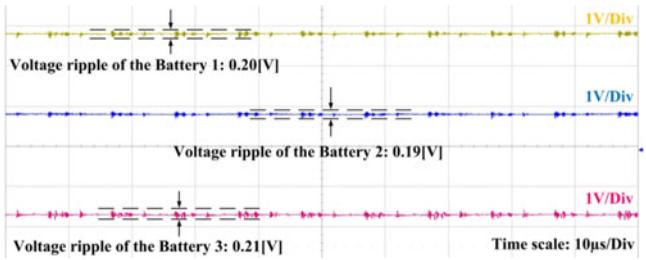

Fig. 15. Output voltage waveforms of the proposed multiple output charger.

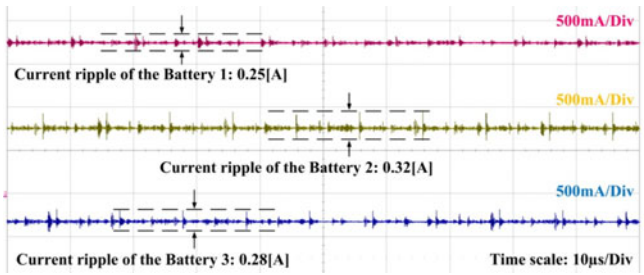

Fig. 16. Output current waveforms of the proposed multiple output charger.

maximum efficiency of the proposed charger is 95.6% at a 90% load.

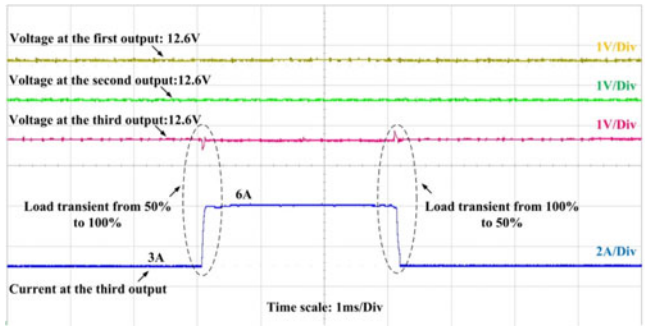

Fig. 17. Transient characteristics of the proposed charger when the load varies from 50% to 100% at one output while 100% load is applied to the other outputs.

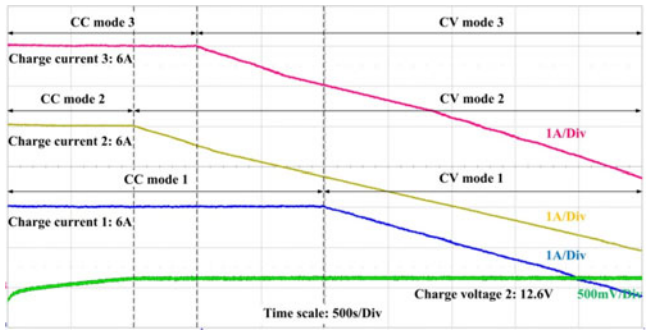

Fig. 18. Charge current profiles of the battery loads by using proposed multiple output charger.

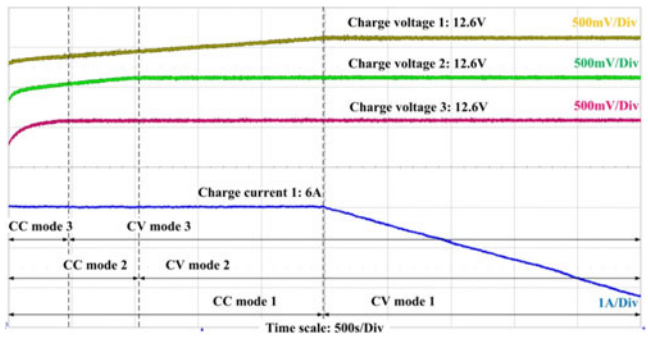

Fig. 19. Charge voltage profiles of the battery loads by using the proposed multiple output charger.

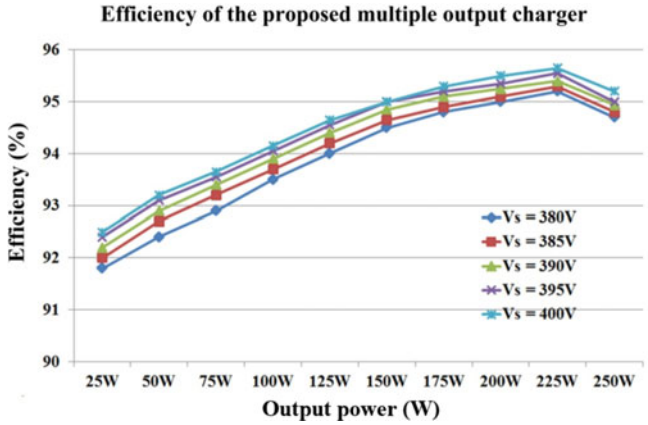

Fig. 20. Efficiency plot of the proposed multiple output charger.

VI. Conclusion

In this paper, a multiple output battery charger based on the TDMC technique is proposed and applied to the phase-shift full-bridge topology to simultaneously charge three Li–Po batteries. The proposed charger can regulate three outputs precisely and independently with only one secondary winding in the transformer. With the help of a digital signal processor capable of high speed operation, the TDMC method can be simply implemented. However, there is a trade-off in the design between the number of outputs and the switching frequency of each output due to the size of the reactive components at the secondary side.

The proposed method offers a simple control technique to achieve an even degree of tight regulation for all of the outputs and can be applied to all kinds of isolated converter topologies. If it is applied to off-board charger applications for the EVs, the installation area can be significantly reduced thereby providing another benefit by decreasing the overall cost of the system.

References

[1] S. Singh, G. Bhuvaneswari, and B. Singh, "Multiple output SMPS with improved input power quality," in *Proc. 2010 Int. Conf. Ind. Inform. Syst.*, Mangalore, Aug. 2010, pp. 382–387.

[2] J. Reddy, G. Bhuvaneswari, and B. Singh, "A single DC-DC converter based multiple output SMPS with fully regulated and isolated outputs," in *Proc. 2005 Annu. IEEE INDICON*, Dec. 2005, pp. 585–589.

[3] A. E. Joy and J. Anudev, "Analysis of multiple output SMPS topology for PC application," *in Proc. 2015 Int. Conf. Comput. Power, Energy Inf. Commuin., Chennai*, Apr. 2015, pp. 0059–0063.

[4] C. D. Technologies, "Charging valve regulated lead acid batteries," *Tech. Note*, C. D. Technol., Blue Bell, PA, USA, 2012.

[5] Emerson Network Power, "Effect of AC ripple current on VRLA battery life," *Tech. Note*, Experts in Business-Critical Continuity, Columbus, OH, USA, 2011. [Online]. Available: http://www.emersonetworkpower.com/

[6] R. J. Wai and J. J. Liaw, "High-efficiency-isolated single-input multiple-output bidirectional converter," *IEEE Trans. Power Electron.*, vol. 30, no. 9, pp. 4914–4930, Sep. 2015.

[7] Y. Zheng, M. Ho, J. Guo, K. L. Mak, and K. N. Leung, "A single-inductor multiple-output auto-buck-boost DC-DC converter with autophase allocation," *IEEE Trans. Power Electron.*, vol. 31, no. 3, pp. 2296–2313, Mar. 2016.

[8] Y.-T. Chen, "Small-signal analysis of a synchronous-switch post regulator with coupled inductor," *IEEE Trans. Ind. Electron.*, vol. 47, no. 1, pp. 55–66, Feb. 2000.

[9] P. Patra, J. Ghosh, and A. Patra, " Control scheme for reduced cross-regulation in single-inductor multiple-output DC–DC converters," *IEEE Trans. Ind. Electron.*, vol. 60, no. 11, pp. 5095–5104, Nov. 2013.

[10] C. Ji, M. Smith, K. M. Smedley, and K. King, "Cross regulation in flyback converters: Analytic model and solution," *IEEE Trans. Power Electron.*, vol. 16, no. 2, pp. 231–239, Mar. 2001.

[11] X. Youhao and P. K. Jain, "A forward converter topology with independently and precisely regulated multiple outputs," *IEEE Trans. Power Electron.*, vol. 18, no. 2, pp. 648–658, Mar. 2003.

[12] B. Su, H. Wen, J. Zhang, and Z. Lu, "A soft-switching post-regulator for multi-outputs dual forward DC/DC converter with tight output voltage regulation," *IET Power Electron.*, vol. 6, no. 6, pp. 1069–1077, Jul. 2013.

[13] S. Chakraborty, A. K. Jain, and N. Mohan, "A novel converter topology for multiple individually regulated outputs," *IEEE Trans. Power Electron.*, vol. 21, no. 2, pp. 361–369, Mar. 2006.

[14] D. Trevisan, P. Mattavelli, and P. Tenti, "Digital control of single-inductor multiple-output step-down DC–DC converters in CCM," *IEEE Trans. Power Electron.*, vol. 55, no. 9, pp. 3476–3483, Sep. 2008.

[15] Z. Shen, X. Chang, W. Wang, X. Tan, N. Yan, and H. Min, "Predictive digital current control of single-inductor multiple-output converters in CCM with low cross regulation," *IEEE Trans. Power Electron.*, vol. 27, no. 4, pp. 1917–1925, Apr. 2012.

[16] J. Sebastian, J. Uceda, M. A. Perez, M. Rico, and F. Aldana, "A very simple method to obtain one additional fully regulated output in zero-current-switched quasiresonant converter," in *Proc. Power Electron. Spec. Conf., San Antonio*, 1990, vol. 21, pp.536–542.

[17] C. Kyusik, P. Joung-Hu, and C. Bo-Hyung, "A novel multiple-output converter using band pass filters," in *Proc. 31st Int. Telecommun. Energy Conf.*, 2009, pp. 1–4.

[18] T. Van-Long and W. Choi, "Novel time division multiple control method for multiple output battery charger," *IEEE Trans. Power Electron.*, vol. 29, no. 10, pp. 5102–5105, Oct. 2014.

[19] T. Van-Long and W. Choi, "Multiple output charger based on phase shift full bridge converter with novel time division multiple control technique," in *Proc. 2014 Int. Power Electron. Conf. (Hiroshima 2014 ECCE-ASIA)*, 2014, pp. 1214–1219.

[20] C. Piao, Z. Li, S. Lu, Z. Jin, and C. Cho, "Analysis of real-time estimation method based on hidden markov models for battery system states of health," *J. Power Electron.*, vol. 16, no. 1, pp. 217–226, Jan. 2016.

[21] T. Zhang, J. Fu, Q. Qian, W. Sun, and S. Lu, "Dead-time for zero-voltage-switching in battery chargers with the phase-shifted full-bridge topology: Comprehensive theoretical analysis and experimental verification," *J. Power Electron.*, vol. 16, no. 2, pp. 425–435, Mar. 2016.

[22] W. Hwa-Young, C. Soo-Yong, S. Young-Min, C. Dae-Taek, and H. Soon-Chan, "Analysis of the lithium battery charge/discharge system using state space averaging method," in *Proc. IEEE 6th Int. Power Electron. Motion Control Conf.*, 2009, pp. 1402–1406.

[23] J. Van Mierlo, P. Van den Bossche, and G. Maggetto, "Models of energy sources for EV and HEV: Fuel cells, batteries, ultracapacitors, flywheels and engine-generators," *J. Power Sources*, vol. 128, pp. 76–89, 2004.

[24] N. B. Hadj-Youssef, K. Al-Haddad, H. Y. Kanaan, and F. Fnaiech, "Small-signal perturbation technique used for DSP-based identification of a three-phase three-level boost-type Vienna rectifier," *Electric Power Appl., IET*, vol. 1, pp. 199–208, 2007.

[25] G. Sen and M. E. Elbuluk, "Voltage and current-programmed modes in control of the Z-source converter," *IEEE Trans. Ind. Appl.,* vol. 46, no. 2, pp. 680–686, Mar.–Apr. 2010.

[26] M. E. Hervas, S. Vazquez, M. Reyes, J. M. Carrasco, and E. Dominguez, "A dual-loop PI controller for a DC/DC full-bridge power converter with ZVS modulation," in *Proc. IEEE 35th Annu. Conf. Ind. Electron.*, 2009, pp. 37–41.

[27] K. Tae-Hoon, L. Seung-Jun, and C. Woojin, "Design and control of the phase shift full bridge converter for the on-board battery charger of electric forklifts," *J. Power Electron.*, vol. 12, pp. 113–119, 2012.

Van-Long Tran was born in Haiphong, Vietnam, in 1988. He received the B.S. degree in electrical engineering from the Hanoi University of Science and Technology, Hanoi, Vietnam, in 2011, and the M.S. degree in electrical engineering from Soongsil University, Seoul, Korea, in 2014.

Since 2014, he has been a Power Supply Researcher at Lutronic Corp., Goyang-si, South Korea. His current research interests include dc–dc converters dealing with the renewable sources and batteries for energy storage system or hybrid electric vehicles, soft-switching techniques for the PWM/pulse-frequency modulation converters, and pulsed power systems for the laser applications.

Hai-Nam Vu was born in Quang Ninh, Vietnam, in 1991. He received the B.S. degree in electrical engineering from the Hanoi University of Technology, Hanoi, Vietnam, in 2014. He is currently working toward the M.S. degree at Soongsil University, Seoul, Korea.

His current research interests include soft-switching dc–dc converter for electric vehicles.

Dai-Duong Tran was born in Hai Phong, Vietnam, in 1988. He received the B.S. degree in electrical engineering from the Hanoi University of Technology, Hanoi, Vietnam, in 2011. He is currently working toward the M.S. degree at Soongsil University, Seoul, Korea.

He was a Research Engineer with Viettel Research and Development Institute, Hanoi, from 2012 to 2014. His current research interests include on-board battery chargers for electric vehicles, soft switching techniques for PWM converters, resonant converter analysis, and control scheme.

Woojin Choi (S'00–M'05) was born in Seoul, Korea, in 1967. He received the B.S. and M.S. degrees in electrical engineering from Soongsil University, Seoul, in 1990 and 1995, respectively, and the Ph.D. degree in electrical engineering from Texas A &M University, College Station, TX, USA, in 2004.

He was a Research Engineer with Daewoo Heavy Industries, Seoul, from 1995 to 1998. In 2005, he joined the School of Electrical Engineering, Soongsil University. His current research interests include modeling and control of electrochemical energy sources, such as fuel cells, batteries, and supercapacitors; power conditioning technologies in renewable energy systems; and dc–dc converters for electric vehicles and fuel cells. He is a Publication Editor of the *Journal of Power Electronics* of the Korean Institute of Power Electronics.

Dr. Choi is an Associate Editor of the IEEE TRANSACTIONS ON INDUSTRY APPLICATIONS.